

Reprinted from

JOURNAL
OF THE
PHYSICAL
SOCIETY
OF
JAPAN



■ FULL PAPER

**A Model for Measured Traveling Waves at End-Diastole
in Human Heart Wall by Ultrasonic Imaging Method**

Naoaki Bekki, Seine A. Shintani, Shin'ichi Ishiwata, and Hiroshi Kanai

J. Phys. Soc. Jpn. **85**, 044802 (2016)

A Model for Measured Traveling Waves at End-Diastole in Human Heart Wall by Ultrasonic Imaging Method

Naoaki Bekki^{1*}, Seine A. Shintani², Shin'ichi Ishiwata¹, and Hiroshi Kanai³

¹*Department of Physics, Faculty of Science and Engineering, Waseda University, Shinjuku, Tokyo 169-8555, Japan*

²*Department of Physics, The University of Tokyo, Bunkyo, Tokyo 113-0033, Japan*

³*Department of Electronic Engineering, Tohoku University, Sendai 980-8579, Japan*

(Received December 24, 2015; accepted January 28, 2016; published online March 4, 2016)

We observe traveling waves, measured by the ultrasonic noninvasive imaging method, in a longitudinal beam direction from the apex to the base side on the interventricular septum (IVS) during the period from the end-diastole to the beginning of systole for a healthy human heart wall. We present a possible phenomenological model to explain part of one-dimensional cardiac behaviors for the observed traveling waves around the time of R-wave of echocardiography (ECG) in the human heart. Although the observed two-dimensional patterns of traveling waves are extremely complex and no one knows yet the exact solutions for the traveling homoclinic plane wave in the one-dimensional complex Ginzburg–Landau equation (CGLE), we numerically find that part of the one-dimensional homoclinic dynamics of the phase and amplitude patterns in the observed traveling waves is similar to that of the numerical homoclinic plane-wave solutions in the CGLE with periodic boundary condition in a certain parameter space. It is suggested that part of the cardiac dynamics of the traveling waves on the IVS can be qualitatively described by the CGLE model as a paradigm for understanding biophysical nonlinear phenomena.

1. Introduction

It is important to measure the rapid motions of the myocardium in the human heart wall during systole and diastole since information on them are useful for the diagnosis of regional myocardial motility.¹⁾ The propagation speed of mechanically excited traveling waves around the aortic-valve closure (AVC) is higher than that of electrically excited waves along the cardiac muscle and the Purkinje fiber around the beginning of the ejection period in the human heart wall.²⁾ Therefore, a study of the measured nonlinear waves due to rapid motions in the cardiac muscle during systole by the ultrasonic imaging method is one of the most interesting subjects in physics and biophysics because there are very few experimental investigations related to biophysical nonlinear phenomena in cardiac systems.^{3,4)}

A phase tracking method with high temporal and spatial resolutions has been developed to measure the rapid velocity in the heart wall by accurately tracking the movement of a point in the heart wall by the constraint least-squares method applied to both the phase and amplitude of quadrature-demodulated signals.⁵⁾ This method that enables the precise measurement of a target velocity for the myocardium plays an important role in characterizing myocardial tissue in terms of systolic properties in vivo, which cannot be obtained by conventional echocardiography (ECG), tissue Doppler imaging, computer tomography, or magnetic resonance imaging.²⁾

The velocity components toward the ultrasonic probe as waveforms and their instantaneous phases were observed by visualizing the propagation of the myocardial response of electric excitation in the human heart wall during systole, which may be modeled by the asymmetric zero-order mode of the Lamb wave.²⁾ These components corresponding to the contraction were generated on the interventricular septum (IVS) at the time of the T-wave of ECG (end-systole), and propagated slowly in the clockwise direction along the left ventricle circumferential direction (x -axis) and beam direction (y -axis) of the ultrasonic probe.

Since small-amplitude pulsive waves on the IVS can be approximated by the Lamb-wave as guided waves⁶⁾ with nonstress-free surfaces, taking into account the effect that the wave energy leaks into the surrounding blood, the Lamb-wave model for traveling pulsive waves on the IVS excited by the AVC at end-systole has been investigated.²⁾ It has been shown that the fundamental properties of small-amplitude traveling waves during systole can be explained by the simple dispersion equation based on the Lamb-wave model, and that the viscoelastic constant of the myocardium in the human heart wall has been estimated by the simple dispersion equation⁷⁾ without using the nonlinear optimization method.²⁾

In the case of large-amplitude pulsive waves on the IVS by the AVC at end-systole, they are nonlinearly modulated in amplitude and phase, and locally generate a phase defect in the IVS of the human heart wall. Strongly modulated pulsive waves with the amplitude dip are created by the generated phase jump, which heteroclinically connects two different patterns back and forth specified by two asymptotic wave-numbers in the longitudinal direction of the IVS from the base to the apex.

However, there are very few nonlinear theoretical models for large-amplitude pulsive waves excited by the rapid motions of the cardiac muscle in the human heart wall. Therefore, to explain the nonlinear behaviors of large-amplitude pulsive waves at the time of the T-wave of ECG (end-systole) in the human heart wall, the one-dimensional complex Ginzburg–Landau equation (CGLE) model has been applied to large-amplitude pulsive waves measured by the ultrasonic noninvasive imaging method.^{8,9)}

The behaviors of modulated propagating pulsive waves at the time of the T-wave of ECG have been observed by the ultrasonic imaging method.^{10–13)} One of the observed phase jumps for one-dimensional traveling waves specified by $\Psi(x, t)$ with a fixed y can be described by the Bekki–Nozaki (BN) hole solutions^{8,9,14,15)} with moving sources in the CGLE,^{16–26)} which is written as

$$\frac{\partial}{\partial t} \Psi = \gamma \Psi + (-p_i + ip_r) \nabla^2 \Psi - (q_i - iq_r) |\Psi|^2 \Psi, \quad (1)$$

where $\Psi(x, y, t)$ denotes a complex scalar function of two-dimensional space (x, y) and time t , and the Laplacian $\nabla^2 \equiv \partial^2/\partial x^2 + \partial^2/\partial y^2$, $p_i < 0$, and $\gamma > 0$ are assumed.

By analyzing the data of traveling pulsive waves on the IVS at end-systole in the lateral direction specified by the x -axis (from the left ventricle to the right ventricle) for a fixed y -axis, it is found that the BN hole solutions¹⁵⁾ in the (1-D) CGLE *heteroclinically* connect two different patterns specified by the asymptotic wavenumbers ($\tilde{q}_1 \neq \tilde{q}_2 \neq 0$) near the phase jump of excited waves. A homoclinic hole,²⁴⁾ on the other hand, is defined in the narrow sense as $\tilde{q}_1 = \tilde{q}_2 \approx 0$.

Traveling pulsive waves on the IVS have been measured by the ultrasonic imaging modality with high spatial and temporal resolutions for healthy young males.^{10–12)} However, the one-dimensional dynamics of large-amplitude traveling waves at the time of the R-wave of ECG (end-diastole) has not been investigated yet. To understand part of the one-dimensional behaviors of the traveling waves in the human heart wall, therefore, a phenomenological model of explanation is at least needed on the basis of the direct measurement of traveling waves at end-diastole by the ultrasonic imaging method.

We show that the behaviors of large-amplitude waves in the longitudinal beam direction (y -axis) at the time of the R-wave of ECG (end-diastole) are different from those of pulsive waves based on the data that were measured in the lateral beam direction of the ultrasonic probe at the time of the T-wave of ECG (end-systole),^{2,8)} and that part of the cardiac dynamics of traveling waves on the IVS at end-diastole can be qualitatively explained by the CGLE model as a paradigm for understanding biophysical nonlinear phenomena.

We present here the one-dimensional CGLE model in the one-dimensional cardiac dynamics for the above waves, which were measured by the ultrasonic imaging method in the longitudinal beam direction (y -axis) from the apex to the base around the time of the R-wave of ECG (end-diastole) on the IVS in the human heart wall, as shown in Fig. 1.

2. Observation of Traveling Waves in Human Heart Wall

By the ultrasonic measurement technique for rapid myocardial motions in vivo, we observed nonlinearly excited waves specified by $\Psi(x, y, t)$ on the IVS around the time of the R-wave of ECG for a healthy young male. We obtained two-dimensional patterns of phase $\Theta(x, y, t)$ and amplitude $|\Psi(x, y, t)|$ of excited waves on the IVS, and their observation time corresponded to $-99.2 \leq t \leq 99.2$ ms during the period from the T-wave to the R-wave of ECG, for at most 0.2 (s). Figure 1 shows a typical snapshot of two-dimensional spatial patterns of phase $\Theta(x, y)$ with $t = 93.25$ ms from the T-wave of ECG in the beam direction from the apex to the base defined by the y -axis set 1,869 points on the IVS and a lateral (scanning) direction to the beam by the x -axis set about 10 points. We can observe a number of phase defects in the two-dimensional spatial phase patterns $\Theta(x, y)$ with a fixed time $t = 93.25$ ms.

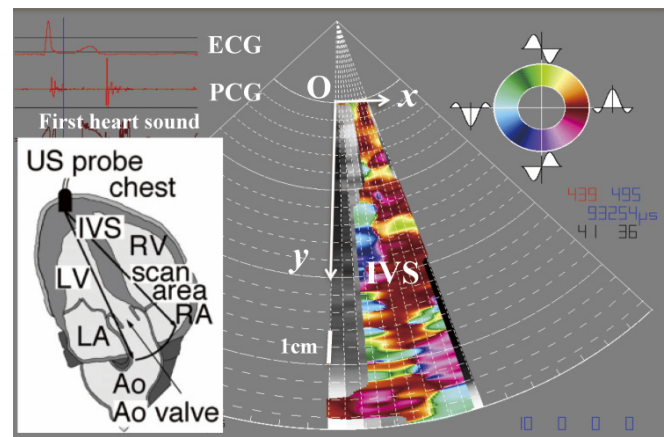


Fig. 1. (Color online) Snapshot of two-dimensional spatial pattern of the phase $\Theta(x, y)$ with a fixed time ($t = 93.25$ ms from the T-wave of ECG) in the 40 Hz component of excited waves on the IVS for a healthy young male, using the ultrasonic measurement technique for myocardial motions in vivo. Point O denotes the origin of the measured 2-D phase plane transformed from the polar coordinate system to the Cartesian coordinate system (x, y) . This spatial pattern is cross-sectional image of the color-coded phase values just after the time of the first heart sound. A phase value at a local point on IVS, for example, changes from cyan ($+180^\circ$) near a certain phase defect, to green ($+90^\circ$), and to red (0°) at a different point and a different time. The left inset shows the scanning range of the ultrasonic beams in this measurement: LV, left ventricle; LA, left atrium; RV, right ventricle; RA, right atrium; US probe, ultrasonic probe; IVS, interventricular septum; Ao, aorta; ECG, electrocardiogram; PCG, phonocardiogram (heart sound).

Figure 2 shows a series of snapshots (a)–(f) of two-dimensional spatial patterns of phase $\Theta(x, y, t)$ for excited waves on the IVS; (a) $t = -5.95$ ms, (b) $t = 13.89$ ms, (c) $t = 33.73$ ms, (d) $t = 53.71$ ms, (e) $t = 73.41$ ms, and (f) $t = 93.25$ ms, from the T-wave of ECG. Many phase defects (y_h) are also observed along the beam line.

Figure 3 shows typical amplitude patterns $|\Psi(y, t)|$ with a fixed x on the IVS in the region of $69 \leq y \leq 95$ mm and $29.8 \leq t \leq 93.25$ ms; Region A, which is shown by a rectangle: $90 \leq y \leq 95$ mm, $29.8 (T_1) \leq t \leq 45.7$ ms (T_2); Region B: $70 \leq y \leq 80$ mm, $t = 53.71$ ms; Region C: $89 \leq y \leq 95$ mm, $t = 83.4$ ms. From these patterns, we can clearly observe traveling amplitude holes in Regions A, B, and C. Since the resolution in the x -axis is lower than that in the y -axis, thereafter, the x -axis (beam number) is fixed. For a fixed x , let us define the measured data of one-dimensional traveling waves around the time of the R-wave of ECG as follows:

$$\Psi(y, t) = |\Psi(y, t)| \exp[i\Theta(y, t)], \quad (2)$$

where y (mm) is directed to the longitudinal axis from the apex to the base on the IVS and the observed time t ($T_1 < t < T_2$, $T_2 - T_1 = 15.9$ ms).

The position of a phase defect is specified by $y = y_h$. By using two different patterns specified by the wavenumbers \tilde{q}_1 and \tilde{q}_2 near y_h , a heteroclinic phase pattern is defined as $\tilde{q}_1 \neq \tilde{q}_2 \neq 0$ at $y = y_h$. For a heteroclinic phase pattern, a pair of asymptotic wavenumbers \tilde{q}_j ($j = 1, 2$) at $y \neq y_h$ is given by

$$\tilde{q}_j = \frac{1}{T_2 - T_1} \int_{T_1}^{T_2} \frac{\Theta(y_2, t) - \Theta(y_1, t)}{y_2 - y_1} dt, \quad (3)$$

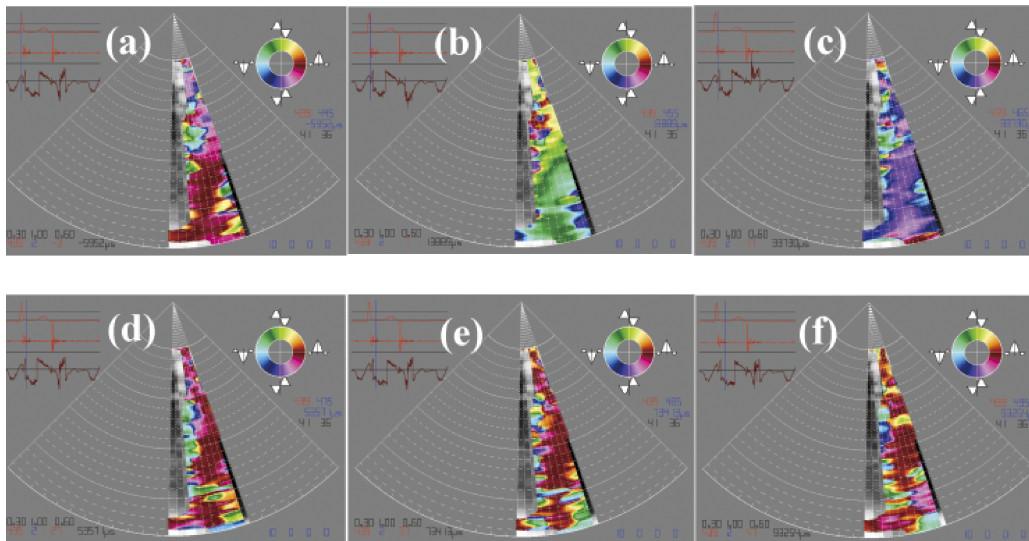


Fig. 2. (Color online) Series of snapshots (a)–(f) of two-dimensional spatial patterns of phase $\Theta(x, y, t)$ for excited waves on the IVS; (a) $t = -5.95$ ms, (b) $t = 13.89$ ms, (c) $t = 33.73$ ms, (d) $t = 53.71$ ms, (e) $t = 73.41$ ms, and (f) $t = 93.25$ ms, from the T-wave of ECG. A number of phase-defects (y_h) are observed along the beam line. Figure 2(f) corresponds to Fig. 1.

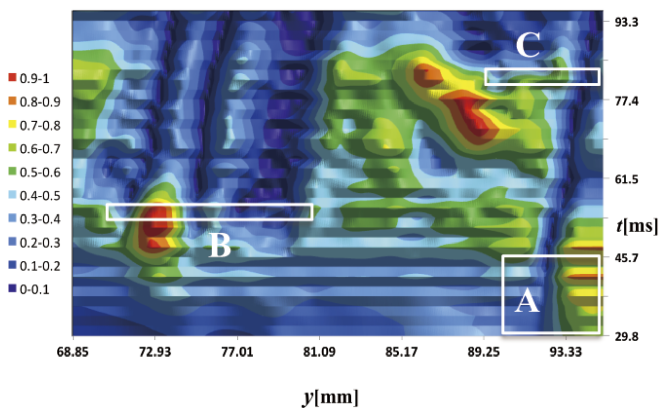


Fig. 3. (Color online) Typical amplitude patterns $|\Psi(y, t)|$ with a fixed x on the IVS measured by the ultrasonic imaging method in the region of $69 \leq y \leq 95$ mm and $29.8 \leq t \leq 93.3$ ms. Region A, which is shown by a rectangle: $90 \leq y \leq 95$ mm, $29.8 \leq t \leq 45.7$ ms; Region B: $70 \leq y \leq 80$ mm, $t = 53.7$ ms; Region C: $89 \leq y \leq 95$ mm, $t = 83.4$ ms.

where \tilde{q}_1 is wavenumber for $y_1 < y_2 < y_h$ and \tilde{q}_2 is wavenumber for $y_h < y_1 < y_2$ during $T_1 < t < T_2$. We also define the phase jump

$$\tilde{\sigma}_{ob} = \limsup_{\epsilon \rightarrow +0} \sup_{y \in \mathbb{R}} |\Theta(y - y_h - \epsilon, t) - \Theta(y - y_h + \epsilon, t)|, \quad (4)$$

where the phase $\Theta(y, t)$ is linearly extrapolated for a fixed time.

Let us also define the position y' of minimum amplitude at the time t' and the position y'' of minimum amplitude at the time t'' ; then, in a uniform linear motion of phase defects, we have its average velocity \tilde{c}_h (mm/ms) defined by

$$\tilde{c}_h = \frac{y'' - y'}{t'' - t'}. \quad (5)$$

As shown in Fig. 3, from Eq. (5), we can obtain that the average velocity of the amplitude hole is about $\tilde{c}_h \approx 0.04 \pm 0.01$ mm/ms.

For a non-heteroclinic phase pattern with a fixed time, on the other hand, from Eq. (3), we obtain a local peak of asymptotic wavenumber \tilde{q}_h at $y = y_h$

$$\tilde{q}_h \propto \frac{\partial \Theta(y, t)}{\partial y}. \quad (6)$$

Using Eqs. (3)–(6) for the observed data, we obtained the following characteristics: (i) a pair of asymptotic wavenumbers $\tilde{q}_1 = \tilde{q}_2 \approx 0$ mm⁻¹ at $y \neq y_h$, which is called a homoclinic hole solution in the CGLE,²⁴ (ii) a local peak of wavenumber $|\tilde{q}_h| \neq 0$ at $y = y_h$ from Eq. (6), (iii) a finite velocity of moving phase defect $|\tilde{c}_h| \neq 0$ mm/ms, and (iv) a phase jump of the homoclinic hole $\tilde{\sigma}_{ob}$ (rad) differs from that of the heteroclinic BN hole at $y = y_h$ in the CGLE.

As shown in Fig. 4, we obtained a local phase profile $\Theta(y, t)$ (rad) near the local point $y_h = 92.4$ mm in Region A: (a) $t_1 = 29.8$ ms, (b) $t_2 = 33.7$ ms, (c) $t_3 = 37.7$ ms, (d) $t_4 = 41.7$ ms, (e) $t_5 = 45.7$ ms. The profile (f) denoted by the broken line is the derivative of the phase profile (e), which corresponds to a local wavenumber obtained from Eq. (6) at $t_5 = 45.7$ ms. We also observed a growing phase defect near y_h in the longitudinal direction for $29.8 \leq t \leq 45.7$ ms and the maximum phase jump $\tilde{\sigma}_{ob} \approx 2.9$ rad for the profile (e). It is clear that two asymptotic wavenumbers \tilde{q}_1 and \tilde{q}_2 at $y \neq y_h$ are small in this region A, that is, $\tilde{q}_1 = \tilde{q}_2 \approx 0$ at $y \neq y_h$, and there exists a local peak of wavenumber $\tilde{q}_h \neq 0$ at $y = y_h$ for a homoclinic phase pattern, as shown in Fig. 4(f). In fact, as shown in Fig. 4(g), the phase profile of Fig. 4(e) ($90 \leq y \leq 95$) at $t_5 = 45.7$ ms can be approximated by

$$\Theta(y, t_5) \approx 1.0 + 1.4 \tanh[(y - y_h)\pi]. \quad (7)$$

The insertion of Eq. (7) into Eq. (6) yields the normalized local wavenumber q_h as

$$q_h(y) \approx \text{sech}^2[(y - y_h)\pi]. \quad (8)$$

This local normalized wavenumber $q_h(y)$ coincides with the curve shown in Fig. 4(f) generated by the phase profile shown in Fig. 4(e). Then, for a traveling plane-wave model in the CGLE,²⁴ we have

$$|\Psi(y, t_5)| \approx \sqrt{1 - q_h(y)^2} \leq 1. \quad (9)$$

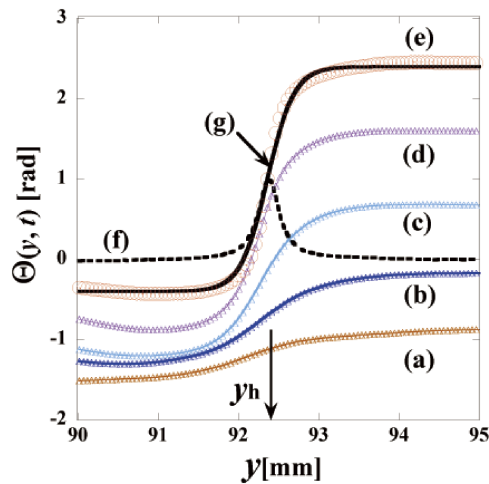


Fig. 4. (Color online) Local phase profile $\Theta(y, t)$ (rad) near the local point $y_h = 92.4$ mm in Region A: (a) $t_1 = 29.8$ ms, (b) $t_2 = 33.7$ ms, (c) $t_3 = 37.7$ ms, (d) $t_4 = 41.7$ ms, and (e) $t_5 = 45.7$ ms (circle). Profile (f) is the normalized derivative of the phase profile (e), which corresponds to a local wavenumber at $t_5 = 45.7$ ms. We can observe a growing phase defect near y_h in the longitudinal beam direction for $29.8 \leq t \leq 45.7$ ms and obtain the maximum phase jump $\tilde{\sigma}_{ob} \approx 2.9$ rad from Eq. (4). Two asymptotic wavenumbers \tilde{q}_1 and \tilde{q}_2 (broken line) at $y \neq y_h$ are small in Region A: $\tilde{q}_1 = \tilde{q}_2 \approx 0$ [see (f)]. The curve (g) (solid line) is given by $\Theta(y, t_5) \approx 1.0 + 1.4 \tanh[(y - y_h)\pi]$. The phase profile of the measurements in the y -axis is quite different from that of the heteroclinic BN hole solutions.

This suggests that the approximated phase profile (7) for Fig. 4(e) qualitatively explains the creation of amplitude holes, which are called *homoclinic holes*. These have been known only as numerical solutions.^{24,27)}

Since the characteristics of these phase profiles are quite different from those of the heteroclinic BN hole solutions in the CGLE, another phenomenological physical model is therefore needed on the basis of the present measurement of traveling waves on the IVS around the time of the R-wave of ECG (end-diastole) for a healthy human heart. These characteristics (i)–(iv) for measured waves on the IVS lead to traveling homoclinic plane waves based on the numerical solutions in the one-dimensional CGLE. Note that we do not know yet the exact solutions for them in the CGLE.²⁷⁾

3. CGLE Model for Traveling Homoclinic Plane Waves

In our case, the scaled one-dimensional CGLE^{16,18,19,21–24,26)} is given by

$$\frac{\partial}{\partial t} \Psi(y, t) = \Psi + (1 + ic_1) \frac{\partial^2}{\partial y^2} \Psi - (1 - ic_3) |\Psi|^2 \Psi. \quad (10)$$

Here, for simplicity, we put the coefficients in Eq. (1) as follows: $c_1 = p_r$, $c_3 = q_r$, $p_i = -1$, $q_i = 1$, and $\gamma = 1$. A set of two parameters, i.e., c_1 and c_3 , in the CGLE (10) determines complex spatiotemporal dynamics due to the Benjamin–Feir instability.²¹⁾

We are interested in the coherent localized structures of excited waves, which are measured noninvasively by the ultrasonic noninvasive imaging method.²⁾ We assume the existence of uniformly propagating solutions of the form in the variable $\xi = y - vt$ for the CGLE;

$$\begin{aligned} \Psi(y, t) &= \hat{\Psi}(y - vt) e^{-i\omega t}, \\ \hat{\Psi}(\xi) &= a(\xi) e^{i\Theta(\xi)}, \end{aligned} \quad (11)$$

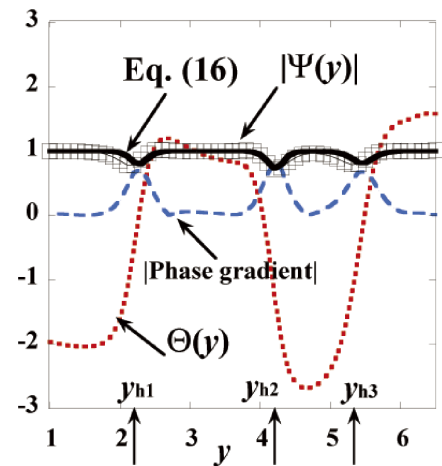


Fig. 5. (Color online) Typical numerical solution of traveling plane wave in the CGLE at $t = 210$: $|\Psi(y)|$ is amplitude (square) and $\Theta(y)$ (rad) the phase (red dotted line) for a local space $1 \leq y \leq 6.5$ (system length $L = 10$) near the position of phase-jumps y_{hk} ($y_{h1} = 2.2$, $y_{h2} = 4.2$, $y_{h3} = 5.4$). The broken line corresponds to the phase gradient $|\hat{q}_{hk}|$ Eq. (15) for the homoclinic phase pattern. The thick solid line can be obtained using Eq. (16) with $\hat{\alpha}_k = 1.2$.

where $a(\xi) \equiv |\hat{\Psi}(\xi)|$, $\Theta(\xi)$, v , and ω denote the amplitude, phase, velocity, and angular frequency, respectively.

The insertion of Eq. (11) into Eq. (10) leads to the following coupled first-order ordinary differential equations:

$$\begin{aligned} \frac{da(\xi)}{d\xi} &= \kappa(\xi) a(\xi), \\ \frac{d\kappa(\xi)}{d\xi} &= -\kappa^2 + q^2 \\ &\quad + \frac{(1 - c_1 c_3) a^2 - 1 - c_1 \omega - v(\kappa + c_1 q)}{1 + c_1^2}, \quad (12) \\ \frac{dq(\xi)}{d\xi} &= -2\kappa q \\ &\quad - \frac{(c_1 + c_3) a^2 - c_1 + \omega - v(c_1 \kappa - q)}{1 + c_1^2}. \end{aligned}$$

Here, we define $\kappa(\xi) = \partial_\xi a/a$ and $q(\xi) = \partial_\xi \Theta$.²²⁾ A family of traveling plane-wave solutions known as coherent structures has been numerically studied using Eq. (12).^{22,24,27)} A homoclinic hole has been defined as an unstable homoclinic orbit associated with a saddle-node bifurcation.^{24,27)} Note that homoclinic holes are not exact solutions of the CGLE (10) and that their numerical solutions are extremely delicate in stability for a parameter space (c_1, c_3, ω, v) .^{22,24,27)}

Homoclinic holes are parameterized by the angular frequency ω and the velocity v , and are numerically observed from Eq. (12) in a certain parameter space.^{24,27)} All the amplitude patterns of the measured excited waves in Fig. 3, however, cannot be explained by homoclinic holes based on Eq. (12) at all. Since numerical solutions of the CGLE in the case of $c_1 c_3 \geq 1$ show chaotic patterns and modulated amplitude waves instead of BN holes and homoclinic holes,^{24,26,27)} therefore, we carried out direct numerical simulations of the CGLE (10) with the condition $c_1 c_3 < 1$.

Figure 5 shows a typical snapshot of numerical solutions in the CGLE with $c_1 = 0.6$ and $c_3 = 1.4$ at $t = 210$ for the local space $1 \leq y \leq 6.5$ near the position of three phase jumps y_{hk} ($y_{h1} = 2.2$, $y_{h2} = 4.2$, $y_{h3} = 5.4$), which may

create almost homoclinic amplitude holes for traveling plane waves. The dotted line denotes the typical spatial phase profile $\Theta(y)$ at $t = 210$. The broken line is the absolute value of the phase gradient $|\hat{q}_{hk}|$ given by Eq. (15), that is, a local peak of wavenumber for the homoclinic phase pattern.^{24,27} We can clearly observe three amplitude holes near y_{hk} ($k = 1, 2, 3$) since each amplitude hole is governed by the phase gradient near the phase jumps. It is suggested that the homoclinic amplitude holes obtained numerically can be approximated by the homoclinic plane-wave solutions.

We have used the fourth-order Runge–Kutta scheme for time and the central-difference scheme for space with periodic boundary condition. The time and space resolutions were $\Delta t = 0.001$ and $\Delta y = 0.1$, respectively, and the system length $L = 10\text{--}500$. The typical initial condition was given as

$$\Psi(y, 0) = ie^{4\pi yi} \tanh[\gamma(y - y_0)],$$

where the constant $\gamma = 0.08$ and $y_0 = L/4$.

One-dimensional phase distribution for a fixed time may be approximately decomposed into small intervals $2\delta_k$ (> 0) in y containing the position of the phase-defect y_{hk} ($1 \leq k \leq n$):

$$\Theta(y) = \bigcup_{k=1}^n \Theta_k, \quad (13)$$

$$\Theta_k = \alpha_k \mathfrak{H}_1 \mathfrak{H}_2 \tanh[\beta_k(y - y_{hk})] + \Theta_k^{(0)}, \quad (14)$$

where $\mathfrak{H}_1 \equiv \mathfrak{H}(y - y_{hk} + \delta_k)$ and $\mathfrak{H}_2 \equiv \mathfrak{H}(y_{hk} + \delta_k - y)$ are the Heviside step functions, and α_k , β_k , and $\Theta_k^{(0)}$ are constant.

From Eq. (14), each normalized local peak of the wavenumber \hat{q}_{hk} near $y = y_{hk}$ may be approximately given as

$$\hat{q}_{hk} = \frac{\partial \Theta_k}{\partial y} = \tilde{\alpha}_k \operatorname{sech}^2[\beta_k(y - y_{hk})], \quad (15)$$

where $\tilde{\alpha}_k$ is a constant that depends on the nonlinear interactions between phase defects. Then, from Eq. (15), we can qualitatively estimate the homoclinic amplitude hole near $y = y_{hk}$,

$$|\Psi_h(y)| \approx \sqrt{1 - \left(\frac{\hat{q}_{hk}}{\hat{\alpha}_k}\right)^2}, \quad (16)$$

where $\hat{\alpha}_k$ is a fitting constant. In fact, as shown in Fig. 5, Eq. (16) can explain the creation of almost homoclinic amplitude holes $|\Psi_h(y)|$ due to the phase jumps at y_{h1} , y_{h2} , and y_{h3} when time is fixed, that is, the numerically obtained amplitude $|\Psi(y)|$ (square symbol) of the CGLE coincides with the homoclinic amplitude hole $|\Psi_h(y)|$ with $\hat{\alpha}_k = 1.2$ (thick solid line).

However, we cannot analytically obtain each magnitude of strongly modulated amplitudes $|\Psi(y)|$ of excited waves since we do not know yet the exact traveling plane-wave solutions of the CGLE [see Fig. 6(f)]. We have shown that Eq. (16) may qualitatively explain the creation of homoclinic plane-wave amplitude holes for measured nonlinear excited waves on the IVS in human heart wall during the period from end-diastole to the beginning of systole by the ultrasonic noninvasive imaging method.

4. Discussion

As shown in Fig. 4, we observed the growing phase defect near $y_h = 92.4$ mm in the longitudinal direction (y -axis) for $29.8 \leq t \leq 45.7$ ms. Then, we obtained the maximum phase

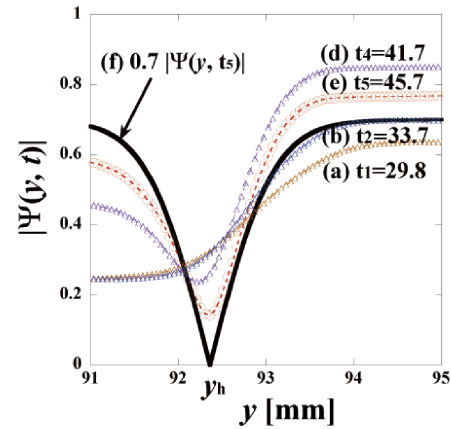


Fig. 6. (Color online) Typical amplitudes $|\Psi(y, t)|$ near the local point $y_h = 92.4$ mm in Region A, which correspond to Figs. 4(a), 4(b), 4(d), and 4(e). Figure 4(c) at $t_3 = 37.7$ ms was omitted to avoid confusion created by a similar curve. A fitting curve for the amplitude profile (e) is shown in (f). We can clearly find homoclinic-type holes near the y_h since the phase defect near y_h creates the amplitude holes [see Fig. 4(f)].

jump from Eq. (4): $\tilde{\sigma}_{ob} \approx 2.9$ rad for Fig. 4(e). The observed two asymptotic wavenumbers \tilde{q}_1 and \tilde{q}_2 at $y \neq y_h$ are small in Region A (Fig. 3): $\tilde{q}_1 = \tilde{q}_2 \approx 0$ [see Fig. 4(f)], which is called a homoclinic hole²⁴ of $|\Psi(y)|$ at $t_5 = 45.7$ ms [Fig. 6(e)]. Figure 6 shows typical amplitudes $|\Psi(y, t)|$ near the local point of phase defect y_h in Region A, which correspond to Figs. 4(a), 4(b), 4(d), and 4(e). Figure 4(c) at $t_3 = 37.7$ ms was abbreviated to avoid confusion with a similar curve. We can clearly observe homoclinic-type holes near y_h since the phase jump near y_h creates the amplitude hole $|\Psi_h(y, t)|$, which decreases and forms a dip shaped like a hole. Namely, the amplitude holes of the measured waves can be qualitatively explained by Eq. (16) with the local wavenumber \hat{q}_{hk} . Note that the phase profile of measured excited waves on the IVS in the y -axis is quite different from that of heteroclinic BN hole solutions.

We show, as in Fig. 7, a snapshot of four phase defects and four non-heteroclinic amplitude holes in Region B (see Fig. 3) near the local points y_k (mm) from left to right ($k = 1, 2, 3, 4$): ($y_1 = 71.4$) mm, ($y_2 = 74.9$) mm, ($y_3 = 76.9$) mm, and ($y_4 = 79.3$) mm. The red dotted line denotes the phase $\Theta(y)$ (rad), the black square symbol stands for the amplitude, and the blue broken line stands for the normalized wavenumber $|\hat{q}_{hk}|$ of the homoclinic phase profile for Region B with a fixed time $t = 53.71$ ms. Since the phase defect at y_k creates the local peak of the wavenumber from Eq. (15) and decreases its amplitude according to Eq. (16), we can find homoclinic-type amplitude holes at ($y = y_k$) mm. Amplitude patterns in Region C can be similarly explained by the same homoclinic plane wave as in Region A and Region B. As shown in Figs. 5 and 7, we find that the phase and amplitude patterns of the measured waves are similar to those of the numerical solutions in the CGLE with periodic boundary condition. This strongly suggests that the dynamics of the measured waves in the longitudinal beam direction on the IVS by the phase tracking method can be qualitatively explained by homoclinic plane-wave numerical solutions in the CGLE for a certain parameter space.

The statistical properties of local structures in defect turbulence for the CGLE have been studied and revealed

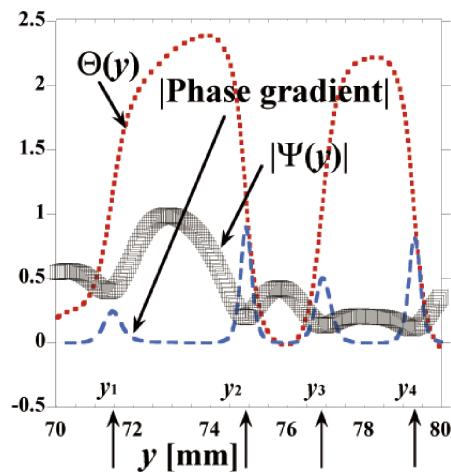


Fig. 7. (Color online) Snapshot of measured four phase jumps and four homoclinic amplitude holes near the local points y_k (mm) from left to right ($k = 1, 2, 3, 4$); $y_1 = 71.4$, $y_2 = 74.9$, $y_3 = 76.9$, and $y_4 = 79.3$. The red dotted line denotes the phase $\Theta(y, t)$ (rad), the black square symbol stands for the amplitude $|\Psi(y)|$, and the blue broken line is the normalized phase gradient $|\hat{q}_{hk}|$ for Region B with a fixed time $t = 53.71$ ms. We can observe four homoclinic-type amplitude holes at $y = y_k$ since each phase jump at y_k creates its corresponding local peak of four wavenumbers.

to be sub-Poisson statistics in the context of birth–death processes.²⁸⁾

5. Conclusions

By the phase-tracking method¹⁰⁾ in ultrasonic diagnostic equipment, we have obtained significant data of excited waves due to mechanical motions during the period from end-diastole to the beginning of systole. We have observed the following main properties of excited waves in the longitudinal beam direction from the apex to the base: (i) two asymptotic wavenumbers $\tilde{q}_1 = \tilde{q}_2 \approx 0 \text{ mm}^{-1}$ for locally homoclinic phase patterns,^{24,27)} (ii) a local wavenumber satisfies the condition $0 < |\hat{q}_{hk}| < 1$, (iii) the velocity of the moving phase defect $|\tilde{c}_h| \neq 0 \text{ mm/ms}$, and (iv) the phase jump $|\tilde{\sigma}_{ob}| \neq 0$ as in Fig. 4.

Let us list the principal results of the present investigation:

- (1) We have observed the two-dimensional phase and amplitude patterns of excited waves on the IVS in a human heart wall.
- (2) We have found that the dynamics of excited waves in the longitudinal beam direction are quite different from those of heteroclinic BN holes in the CGLE since the asymptotic wavenumbers satisfy $\tilde{q}_1 = \tilde{q}_2 \approx 0$ at $y \neq y_h$.
- (3) We have carried out numerical simulations of traveling plane-wave solutions in the CGLE with $c_1 c_3 < 1$ under the periodic boundary condition.
- (4) We have shown that the observed cardiac dynamics of the traveling waves in the longitudinal beam direction on the IVS can be qualitatively explained by the numerical homoclinic plane-wave solutions in the CGLE.

- (5) We expect that the CGLE model for measured traveling waves in the human heart wall plays an important role in understanding the phenomenon of sarcomeric oscillations such as spontaneous oscillatory contraction (SPOC)²⁹⁾ and hyperthermal sarcomeric oscillations (HSOs)³⁰⁾ occurring in cardiac muscles at an intermediate activation level.
- (6) We hope that our fundamental study may be useful for characterizing and quantifying normal and pathological hearts (ischemia and infarction) in vivo, using myocardial elastography, since the propagation speed of contraction waves in a healthy heart is different from that in a pathological one.³¹⁾

*n.bekki@kurenai.waseda.jp

- 1) H. Kanai and Y. Koiwa, *Ultrasound Med. Biol.* **27**, 481 (2001).
- 2) H. Kanai, *IEEE Trans. Ultrason. Ferroelectr. Freq. Control* **52**, 1931 (2005).
- 3) R. A. Gray, O. A. Mornev, J. Jalife, O. V. Aslanidi, and A. M. Pertsov, *Phys. Rev. Lett.* **87**, 168104 (2001).
- 4) S. Takagi, A. Pumir, L. Kramer, and V. Krinsky, *Phys. Rev. Lett.* **90**, 124101 (2003).
- 5) H. Kanai, M. Sato, Y. Koiwa, and N. Chubachi, *IEEE Trans. Ultrason. Ferroelectr. Freq. Control* **43**, 791 (1996).
- 6) T. Kundu, *Ultrasonic Nondestructive Evaluation* (CRC Press, New York, 2003) p. 223.
- 7) N. Bekki and S. A. Shintani, *J. Phys. Soc. Jpn.* **84**, 124802 (2015).
- 8) N. Bekki, Y. Harada, and H. Kanai, *J. Phys. Soc. Jpn.* **81**, 073801 (2012).
- 9) N. Bekki, Y. Harada, and H. Kanai, *AIP Conf. Proc.* **1493**, 96 (2012).
- 10) H. Kanai, *Ultrasound Med. Biol.* **35**, 936 (2009).
- 11) K. Nakahara, H. Hasegawa, and H. Kanai, *Jpn. J. Appl. Phys.* **53**, 07KF09 (2014).
- 12) M. Tanaka, T. Sakamoto, S. Sugawara, Y. Katahira, H. Tabuchi, H. Nakajima, T. Kurokawa, H. Kanai, H. Hasegawa, and S. Ohtsuki, *J. Cardiol.* **63**, 313 (2014).
- 13) S. Miyashita, J. Murotsuki, J. Muromoto, K. Ozawa, N. Yaegashi, H. Hasegawa, and H. Kanai, *Ultrasound Med. Biol.* **41**, 1311 (2015).
- 14) K. Nozaki and N. Bekki, *J. Phys. Soc. Jpn.* **53**, 1581 (1984).
- 15) N. Bekki and K. Nozaki, *Phys. Lett. A* **110**, 133 (1985).
- 16) N. Bekki, *J. Phys. Soc. Jpn.* **50**, 659 (1981).
- 17) K. Nozaki and N. Bekki, *Phys. Rev. Lett.* **50**, 1226 (1983).
- 18) K. Nozaki and N. Bekki, *Phys. Rev. Lett.* **51**, 2171 (1983).
- 19) Y. Kuramoto, *Chemical Oscillations, Waves, and Turbulence* (Springer, Berlin, 1984) Springer Series in Synergetics, Vol. 19.
- 20) K. Nozaki and N. Bekki, *Physica D* **21**, 381 (1986).
- 21) H. Chaté and P. Manneville, *Phys. Lett. A* **171**, 183 (1992).
- 22) W. van Saarloos and P. C. Hohenberg, *Physica D* **56**, 303 (1992).
- 23) M. C. Cross and P. C. Hohenberg, *Rev. Mod. Phys.* **65**, 851 (1993).
- 24) M. van Hecke, *Phys. Rev. Lett.* **80**, 1896 (1998).
- 25) J. Lega, *Physica D* **152–153**, 269 (2001).
- 26) I. S. Aranson and L. Kramer, *Rev. Mod. Phys.* **74**, 99 (2002).
- 27) M. van Hecke, *Physica D* **174**, 134 (2003).
- 28) Y. Uchiyama and H. Konno, *Phys. Lett. A* **378**, 1350 (2014).
- 29) S. Ishiwata, Y. Shimamoto, and N. Fukuda, *Prog. Biophys. Mol. Biol.* **105**, 187 (2011).
- 30) S. A. Shintani, K. Oyama, N. Fukuda, and S. Ishiwata, *Biochem. Biophys. Res. Commun.* **457**, 165 (2015).
- 31) E. E. Konofagou, S. Fung-kee-Fung, J. Luo, and M. Pernot, *Proc. 28th IEEE EMBS Annu. Int. Conf.*, 2006, p. 3348.